Renewable Energy 145 (2020) 2056–2073

Contents lists available at ScienceDirect

Renewable Energy

journal homepage: www.elsevier.com/locate/renene

Curved vs. flat solar air heater: Performance evaluation under diverse environmental conditions

Ajeet Pratap Singh, O.P. Singh*

Department of Mechanical Engineering, Indian Institute of Technology (BHU), Varanasi, UP 221005, India

ARTICLE INFO

Article history:
Received 13 March 2019
Received in revised form
4 July 2019
Accepted 19 July 2019
Available online 22 July 2019

Keywords:
Solar air heater
Windward and leeward
Aerodynamic
Thermal performance
CFD

ABSTRACT

The present study evaluates and compares the performance matrix of a curved and flat solar air heater (SAH) under diverse environmental conditions using an experimentally validated numerical model. Firstly, the optimum curvature angle for curved SAH that offers optimum thermal performance (i.e. 25°) under wide range of parameters such as Reynolds numbers (2200–6000), mass flow rate (0.0172 −0.0472 kg/sm^2) and solar radiation inclination angle (0–60°) has been determined. The enhancement factor (i.e. Nu_{curved}/Nu_{flat}) is in the range 1.5-2.2 which show that curved SAH is thermally much better than flat design. Secondly, the optimized curved SAH is then compared with flat design for 0–60° tilt angles(θ), under tranquil and windy conditions (wind velocity range: 0.5–4 m/s), respectively. Under windy condition the heat loss from SAH to surrounding is lower for curved SAH at $\theta = 0°$, 60° in windward, 30° in leeward and 30° in tranquil- condition in comparison to flat SAH. In the extreme case $\theta = 60°$ and wind speed of 4 m/s, the percentage change in average differential pressure coefficient ΔC_P is about 2% higher for curved SAH under windward while it is about 19% less in leeward condition compared to flat SAH.

1. Introduction

Efficient conversion of solar energy into useful energy is going to be the biggest challenge for the human race as other non-renewable resources of energy are getting scarce day by day. At the same time, it provides a unique opportunity to improve the designs to meet the future growing needs. For low- and moderate-temperature applications such as active building heating, air conditioning, drying process etc., solar air heater (SAH) is the best suited device [1–4]. Apart from high thermal efficiency, proper integration of SAH with the heating, ventilation, and air conditioning (HVAC) system is also considered as an important critical factor [5–9].

A recent study [10] demonstrated that curved SAH shows significant improvement in terms of thermal efficiency. The authors presented various avenues for thermal efficiency improvement such as using internal ribs of various shape and sizes. However, there remains many questions to be answered. Some important questions that needs to be addressed are: (a) what is the optimum curvature angle for which the thermal efficiency is maximized?, (b) How the optimized curved SAH perform vis-à-vis conventional flat SAH under various environmental condition? and (c) How the efficiency of SAH depends on different environmental wind conditions. Scientific literature addressing above issues are scarce.

The curved solar panel shown in Fig. 1(a), showed significant increase in the outlet air temperature and hence Nusselt number compared to flat plate SAH [11,12,29]. The authors [12] used the curved panel with curvature angle of 30.94° to enhance the thermal characteristics of SAH. We first developed a computational fluid dynamics (CFD) model of this design and validated the results for various heat fluxes and mass flow rates. In the second stage, we optimized the curvature angle for best efficiency. The modification in the curvature angle in the range of 22°–40° with an increment of 1° in curvature angle have been reported. For a curved SAH, 19 different curvature angles were studied. The objective is to investigate the best curvature angle and effect of various design changes on thermal performance under different mass flow rate (m) and solar radiation angle w.r.t. normal to the absorber plate (θ_i). We have also reported the transient thermal performance to determine how quickly the SAH respond before attaining the steady state condition. This is important especially in the design selection when a new curved design is compared with the traditional flat plate

* Corresponding author.
E-mail address: opsingh.mec@iitbhu.ac.in (O.P. Singh).

https://doi.org/10.1016/j.renene.2019.07.090
0960-1481/

Nomenclature

A_p	area of absorber plate, m^2
H	duct height, mm
L	length of solar air heater, mm
W	width of solar air heater, mm
D_H	hydraulic diameter, mm
D_e	equivalent diameter, mm
SAH	solar air heater
CPSP	curved plate single pass flow solar air heater
R_c	curvature radius of the path of the curved channel of SAH, mm
V	velocity of air, m/s
h	convective heat transfer coefficient, W/m^2K
I	solar insolation, W/m^2
C_p	specific heat of air at constant pressure, J/kg K
k_a	thermal conductivity of air, W/m K
k_g	thermal conductivity of glass, W/m K
k_i	thermal conductivity of insulation, W/m K
t_i	thickness of the insulation, mm
m	mass flow rate, kg/sm^2
ΔP	pressure drop, N/m^2
N	number of glass cover
Pr	Prandtl number
Q_u	useful heat gain, J
Nu	Nusselt number
Re	Reynolds number
D_n	Dean number
U_b	back heat loss coefficient, W/m^2K
U_t	top heat loss coefficient, W/m^2K
U_l	overall heat loss coefficient, W/m^2K
U_s	side heat loss coefficient, W/m^2K
T_o	outlet temperature of air, K
T_i	inlet temperature of air, K
T_{pm}	mean temperature of absorber plate, K
f	friction factor
C_{tp}	total pressure coefficient
C_P	pressure coefficient
P_t	pressure of top glass surface of SAH, N/m^2
P_b	pressure of bottom surface of SAH, N/m^2
V_∞	freestream velocity of air, m/s
ΔC_P	Streamwise differential pressure coefficient, $\frac{(P_t - P_b)}{\frac{1}{2}\rho V_\infty^2}$
EF	heat transfer enhancement factor (Nu_{curved}/Nu_{flat})

Greek symbols

ε_g	emissivity of glass cover
ε_p	emissivity of absorber plate
η_{th}	thermal efficiency of SAH
ρ	density of air, kg/m^3
α	absorptivity of absorber plate
θ	tilt angle (angle between normal to curved SAH and vertical Y-axis), °
θ_i	solar radiation (insolation) inclination angle w.r.t. normal to the absorber plate of SAH, °
τ	transmisivity of glass cover
μ	dynamic viscosity of air, Ns/m^2
$(\tau\alpha)$	transmittance-absorbent product of glass cover

design.

Although there have been several studies that reports performance evaluation of a flat plate SAH under different environmental conditions [13,14], however, scientific literature that evaluate and compares the performance of a curved SAH with the flat SAH under various conditions are scarce. These important issues have been addressed in the paper. The second and third issue we have addressed here is that how the optimized curved solar air heater performs under environmental wind conditions and its assessment with conventional flat SAH. Wind induced heat loss significantly affect the efficiency of the solar components [13]. Since the geometry of curved and flat plate air heaters are different, it is expected that wind induced heat loss from different directions would vary significantly and hence the thermal performance. Dominant mode of heat transfer from the surface is convection heat transfer. Hence, heat loss from the surface is generally investigated in terms of heat transfer coefficient or the non-dimensional Nusselt Number (i.e. ratio of convective heat transfer to conductive heat transfer, $Nu = h D_e/k$). In this paper, we have reported the local Nusselt number variation along the surface of both curved and flat plate under environmental wind conditions. To study this, we first developed the computational model of the experimental setup (see Fig. 1(b)) for a flat panel reported by Wu et al. [13]. Results were validated with the reported data under environmental wind conditions. Other details have been presented in the subsequent sections.

Apart from thermal efficiency, aerodynamic characteristics of the solar collectors also plays a vital role in making decisions during its installation [15–19]. Drag and lift forces resulting from aerodynamic effects caused by maneuvering winds acting on the standalone solar panels can cause substantial damage, thereby reducing their operational efficiency and possibly creating the need for costly maintenance or replacement unless properly accounted for during the design process [18–23]. Hence, it is imperative to investigate aerodynamics loading of the design. Which type of collector performs better: Curved or flat? Scientific literature is also scarce on this aspect of solar collector performance study. Pressure coefficient under windy conditions have been reported and compared in detail.

Data reported in this paper would help in making informed decisions on the selection of type of solar collectors for different applications. The paper is organized as follows: In section 2, details of computational model with boundary conditions has been presented. The section 3, comprises of details about incident solar radiation on the curved SAH and its thermal efficiency. Section 4, explains the selection of turbulence model and validation of CFD (computational fluid dynamics) model. The results and discussion is described in section 5 followed by conclusions in section 6.

2. The computational model

Fig. 2 shows the designs of SAH indicating different solar inclination angle, various parts, and the direction of wind for windward and leeward orientation. Mesh generation and suitable boundary conditions were imposed on the domain as discussed in the following subsections.

2.1. Design procedure for optimum curvature angle

The SAH comprises of an inlet and outlet section, top glass surface and insulated bottom [10]. The surface areas of curved and flat SAH were kept same. The curved length is1600 mm and the opening height (i.e. distance between top glass surface and insulated bottom) is 40 mm. These dimensions also same for flat SAH.

Fig. 1a. Experimental set up [11].

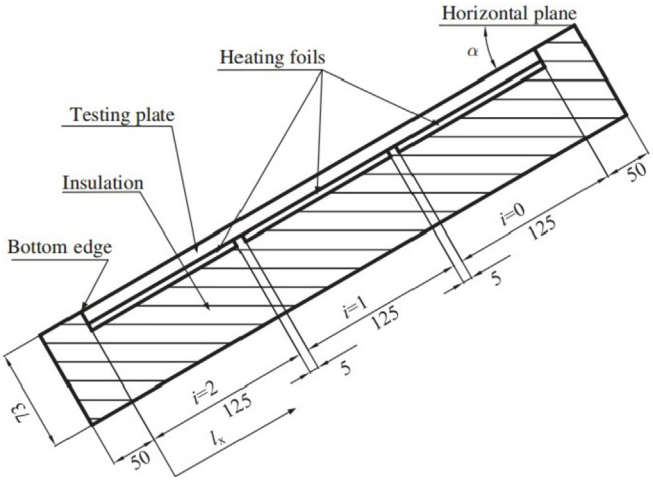

Fig. 1b. Experimental set up [13].

The experimental analysis of a curved SAH having same dimensions with 30.94° curvature angle was reported (shown in Fig. 1(a)) [12]. The effects of different curvature angle in the range of 22°–40° of a curved SAH on the thermal characteristics i.e. outlet air temperature (T_o) and Nusselt number (Nu) (i.e. ratio of convective heat transfer to conductive heat transfer, $Nu = h\,D_e/k$) at different values of solar radiation angle (refer Fig. 2(a)) are reported numerically in the present study. Here, D_e is the equivalent diameter of the cross-section. Table 1 shows the range of parameters for the SAH performance investigations.

The details of parameters considered in the present study are mentioned in Table 1.

2.2. Procedure for environmental wind effect study on curved SAH

The model of a curved solar air heater having an optimum curvature angle has been placed inside the wind tunnel. The wind tunnel is designed in such a way not to interrupt the flow by the walls of the tunnel. The length, width and height of the wind tunnel considered in the present study is shown in Fig. 3(a). Inside the wind tunnel, a curved SAH having 25° i.e. optimum curvature angle comprises of a glass glazing (3 mm thick) placed at 20 mm distance above the absorber plate and distance between absorber plate and bottom insulation is 40 mm [12] as shown in Fig. 2(b). The heat transfer analysis of curved and flat SAH have been performed at various tilt angle 'θ' whose values are 0°, 15°, 30°, 45°, and 60° at both windward (X*OY plane) and leeward (XOY plane) orientation as shown in Figs. 2(c), 3(b) and (c). The Nusselt number for the considered cases have been calculated at the surface of the top glass plate of the SAH. The Nusselt number (Nu) (i.e. ratio of convective heat transfer to conductive heat transfer, $Nu = h\,L_c/k$, where L_c is the length of the glass plate) at different values of SAH tilt angle. The results of curved SAH have been further compared with the flat SAH.

2.3. Mesh generation and grid independence study

Fig. 4 shows the meshed region of the curved SAH. Fine meshed regions near the surfaces are also shown. Since the boundary layer formation, swirl motion and secondary flow vortices are confined near to the SAH surfaces, very fine meshes were necessary around these regions.

2.4. Grid independent test of a curved SAH for thermal performance

The optimum number of mesh elements were considered after performing grid independence test. In the grid independent test, curved SAH having 25° curvature angle has been tested for number of elements in the range of 10923–32004 under same set of boundary conditions. The percentage variation in Nusselt number (Nu) are calculated and shown in Table 2. It is 0.0038%, 0.036%, and 0.023% when number of elements increases from 10923 to 13937, 13937 to 20489 and 20489 to 32004, respectively. Since the variations in results is insignificant, the number of elements selected as 32004 for all further simulation.

2.5. Grid independent test of a curved SAH for environmental wind condition

In the grid independent test, the tunnel comprises of a curved SAH having 25° curvature angle has been tested for number of elements in the range of 66422–86759 for environmental wind velocity of 2 m/s under constant heat flux of 800 W/m^2 assigned to top absorber surface and boundary conditions were same for all cases. The percentage variation of Nusselt number (Nu) were calculated are shown in Table 3. The percentage variation of Nusselt number (Nu) were 0.474%, 0.519%, and 0.298% when number of elements increases from 66422 to 66439, 66439 to 72596 and 72596 to 86759, respectively. Since the variations in results is insignificant, the number of elements selected as 86759 for all further simulation.

2.6. Boundary conditions

2.6.1. Boundary condition to find best curvature angle of a curved SAH

The inlet of SAH was assigned to mass flow inlet (mass flux of air, kg/s.m^2) and pressure outlet (i.e. standard surroundings pressure

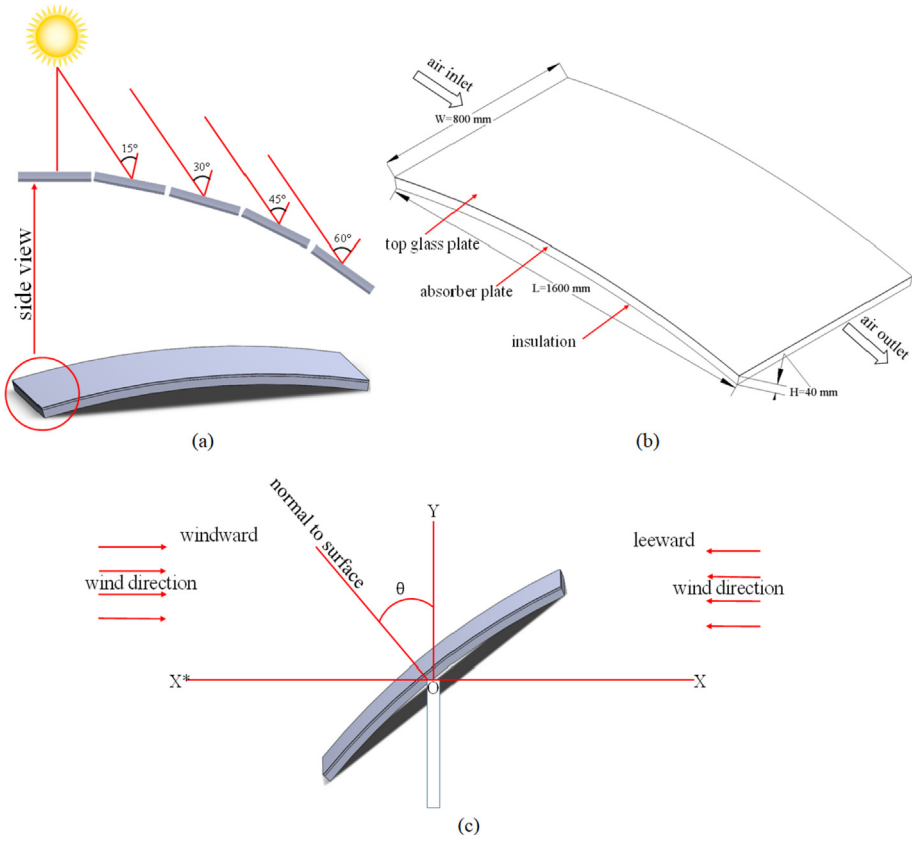

Fig. 2. Design description of the curved SAH model. (a) solar insolation on a curved SAH at different angles, (b) dimensions of the curved SAH geometry, (c) wind direction representation w.r.t. tilt angle (θ) of SAH.

Table 1
Range of parameters.

S. No.	Parameters	Parametric values
1	Reynolds number	2209, 3722, 6058
2	Mass flow rate (kg/s.m^2)	0.0172, 0.029, 0.0472
3	Curvature angle	22°–40° (step size 1°)
4	Solar radiation angle (θ_i) and tilt angle (θ)	0°, 15°, 30°, 45°, 60°
5	Wind velocity (m/s)	0.5, 1, 2, 3, 4

chosen as reference) condition at outlet section. Top wall (curved absorber plate) of domain was exposed to uniform heat flux at different solar radiation inclination angle (θ_i) i.e. 0°, 15°, 30°, 45°, and 60° w.r.t. normal to plane of the absorber plate (see Fig. 2(a)). All other surfaces were kept as adiabatic i.e. assuming ideal conditions to mimic experimental situation [10]. Simulations were performed for unsteady case and value of variables such as Nusselt number, outlet temperature etc. were extracted when their values become invariant with time.

2.6.2. Boundary condition to study the effect of environmental wind condition

The curved SAH has been placed inside the wind tunnel, the tunnel inlet section was set to air velocity (m/s) at inlet and outlet section as pressure outlet (standard ambient pressure taken as reference). The no-slip boundary condition was assigned to top and bottom wall of the wind tunnel. The top absorber plate of curved SAH was exposed to constant heat flux and rest surfaces were kept as adiabatic wall which is similar to the experimental conditions where these surfaces are insulated to avoid heat exchange with the surroundings. The SAH tilted to different tilt angles 'θ' whose values are 0°, 15°, 30°, 45°, and 60°, each case has been tested under wind velocity of 0.5, 1, 2, 3, and 4 m/s, respectively for both windward and leeward orientation under steady state condition (see Fig. 3(c)). All thermophysical properties of air is assumed to be constant as rise in air temperature is insignificant and listed in Table 4.

2.7. Physical models and sets of governing equations

Finite volume technique (FVM) has been used to discretize the two-dimensional computational flow domain for further analysis using commercial HyperWorks software. The flow domain has been exposed to necessary boundary conditions as mentioned before. The continuity, momentum and energy equations for the flow domain were solved using time marching technique. The pressure and velocity field have been solved using SIMPLE (semi-implicit method for pressure linked equations) algorithm. The convergence criteria were of the order of 10^{-5} order for velocity component and momentum equation and 10^{-3} for energy equation.

Continuity equation

$$\frac{\partial u}{\partial x}+\frac{\partial v}{\partial y}=0 \tag{1}$$

Momentum equations

$$\rho\left[\frac{\partial u}{\partial t}+\frac{\partial(uu)}{\partial x}+\frac{\partial(uv)}{\partial y}\right]=-\frac{\partial p}{\partial x}+\frac{\partial}{\partial x}\left[(\mu+\mu_t)\frac{\partial u}{\partial x}\right]+\frac{\partial}{\partial y}\left[\times(\mu+\mu_t)\frac{\partial u}{\partial y}\right]-\frac{2}{3}\rho\frac{\partial k}{\partial x} \tag{2}$$

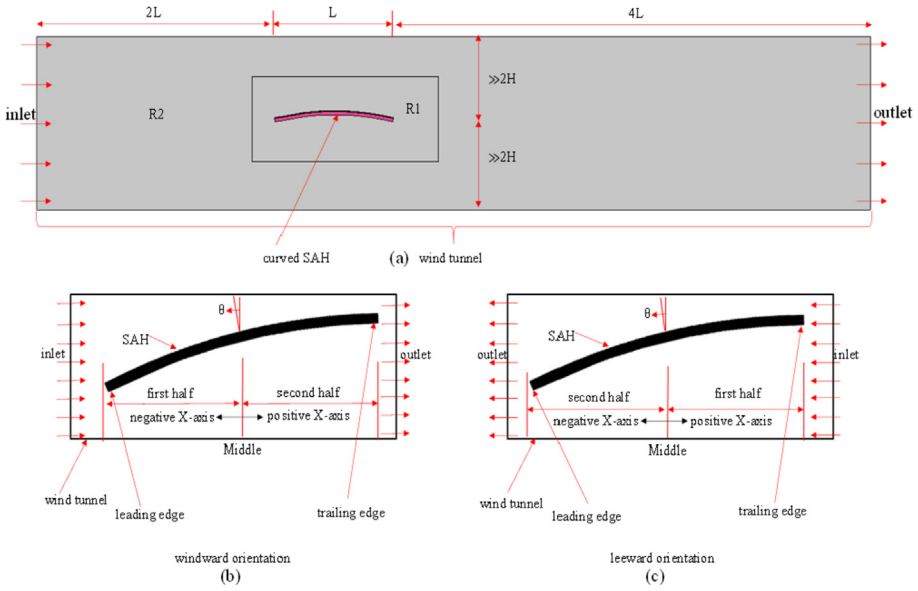

Fig. 3. Design description of various geometric parameters to determine the effects of environmental wind conditions on SAH. (a) wind tunnel design specification, (b) windward orientation, (c) leeward orientation.

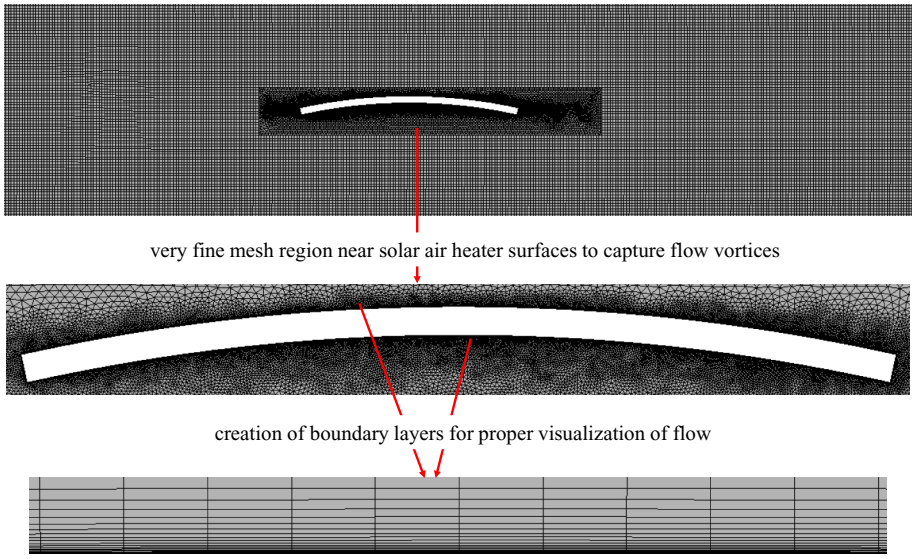

Fig. 4. Mesh of computational flow domain of the curved SAH in a wind tunnel.

Table 2
Grid independent test of a curved SAH.

S. No.	Number of elements	Percentage variation in Nusselt number (*Nu*)
1	10923	–
2	13937	0.0038
3	20489	0.036
4	32004	0.023

Table 3
Grid independent test of environmental wind effect on the curved SAH.

S. No.	Number of elements	Percentage variation in Nusselt number (*Nu*)
1	66422	–
2	66439	0.474
3	72596	0.519
4	86759	0.298

$$\rho\left[\frac{\partial v}{\partial t}+\frac{\partial(uv)}{\partial x}+\frac{\partial(vv)}{\partial y}\right]=-\frac{\partial p}{\partial y}+\frac{\partial}{\partial x}\left[(\mu+\mu_t)\frac{\partial v}{\partial x}\right]+\frac{\partial}{\partial y}\left[(\mu+\mu_t)\frac{\partial v}{\partial y}\right]-\frac{2}{3}\rho\frac{\partial k}{\partial y}-\rho g \quad (3)$$

Energy equation

$$\rho\left[\frac{\partial T}{\partial t}+\frac{\partial(uT)}{\partial x}+\frac{\partial(vT)}{\partial y}\right]=\frac{\partial}{\partial x}\left[\left(\frac{K}{C_P}+\frac{\mu_t}{Pr_t}\right)\frac{\partial T}{\partial x}\right]+\frac{\partial}{\partial y}\left[\left(\frac{K}{C_P}+\frac{\mu_t}{Pr_t}\right)\frac{\partial T}{\partial y}\right] \quad (4)$$

where μ_t is the turbulent viscosity, k is the kinetic energy of turbulence and Pr_t is the turbulent Prandtl number.

Reynolds number

Table 4
Thermo-physical properties of air at 300 K.

Properties name	Value
Dynamic viscosity (μ)	1.855×10^{-5} N/m^2
Thermal conductivity (k)	0.026 W/m K
Prandtl number (Pr)	0.71
Specific heat (C_p)	1003.62 J/kg K
Density (ρ)	1.184 kg/m^3

$$Re = \frac{Inertia\ force}{Viscous\ force} = \frac{\rho\, v D_e}{\mu} \tag{5}$$

Dean number

$$D_n = Re\sqrt{\frac{D_H}{R_C}} \tag{6}$$

where, $D_H = \frac{H}{2}$ i.e. half opening height of the SAH duct. Other constants in the equations have usual meaning.

In our case, since the values of D_n and Re are of the range 180–494 and 2209–6058 respectively, which falls under turbulent flow range [12,24], and hence turbulent flow models are used for the investigations.

2.8. Comparative assessment of globally received solar radiation on flat and curved SAH

It has been shown by the same authors [10,29] that for small curvature angles, incident solar radiation received by a curved and flat plate SAH are of the same order. Hence, curvature effect on the received global solar radiations would not be affected. Hence, same heat flux is imposed on the curved and flat SAH for the investigation. It has also been shown experimentally [12] that similar conditions prevail in the curved and flat SAH.

3. Thermal efficiency

Same expression for thermal efficiency, η_{th} is used for curved and flat SAH performance comparation. The parameters for thermal efficiency calculation requires solar insolation, heat energy gained by the flowing air and various heat losses to environment. Expression for η_{th} is given by Refs. [25,26],

$$Q_u = F_R A_p [I(\tau\alpha) - U_l(T_o - T_i)] \tag{7}$$

Here, F_R is the collector heat-removal factor, A_p is the absorber plate area, U_l is overall heat loss coefficient, $(\tau\alpha)$ is transmittance-absorbent product of glass cover. Expression for F_R is given by,

$$F_R = \frac{\dot{\mathbf{m}}\, C_p}{U_l A_p}\left[1 - exp\left\{-\frac{F' U_l A_p}{\dot{\mathbf{m}}\, C_p}\right\}\right]$$

where F' is the collector efficiency factor.

$$F' = \left(1 + \frac{U_l}{h}\right)^{-1}$$

The expression for bottom loss (U_b), side loss (U_s) and top loss (U_t) coefficients are given as:

$$U_b = \frac{k_i}{t_i} \qquad and \qquad U_s = \frac{(L+W)Hk_i}{LWt_i} \tag{10}$$

$$U_t = \left[\frac{M}{\left(\frac{C}{T_{pm}}\right)\left(\frac{T_{pm}-T_a}{M+f}\right)^{0.33}} + \frac{1}{h_w}\right]^{-1} + \left[\frac{\sigma\left(T_{pm}^2 + T_a^2\right)(T_{pm}+T_a)}{\frac{1}{\varepsilon_p + 0.05M(1-\varepsilon_p)} + \frac{(2M+f-1)}{\varepsilon_c} - M}\right] \tag{11}$$

where $f = (1 - 0.04\, h_w + 0.0005\, h_w^2)(1 + 0.091\, M)$

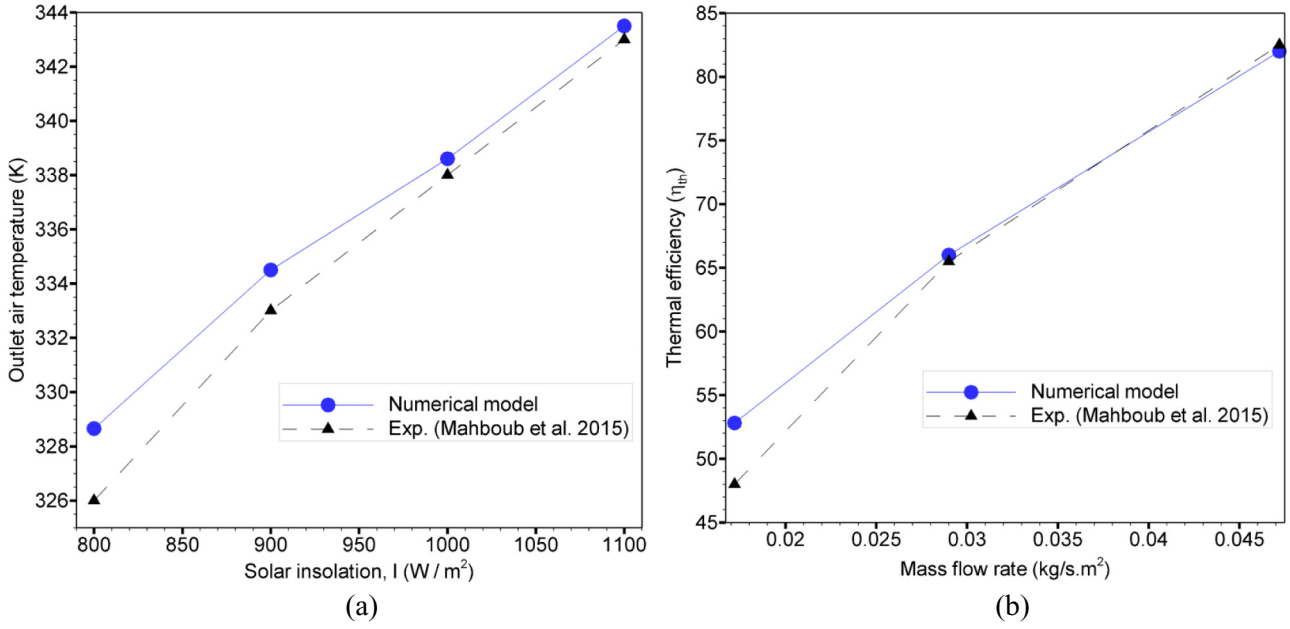

Fig. 5. (a) Variation of outlet air temperature (T_o) of a curved plate SAH w.r.t. constant value of absorber heat flux (W/m^2) at mass flow rate m = 0.0172 kg/s.m^2; (b) Variation in thermal efficiency at mass flow rate in the range of 0.0172–0.0472 kg/s.m^2 at constant heat flux of 800 W/m^2.

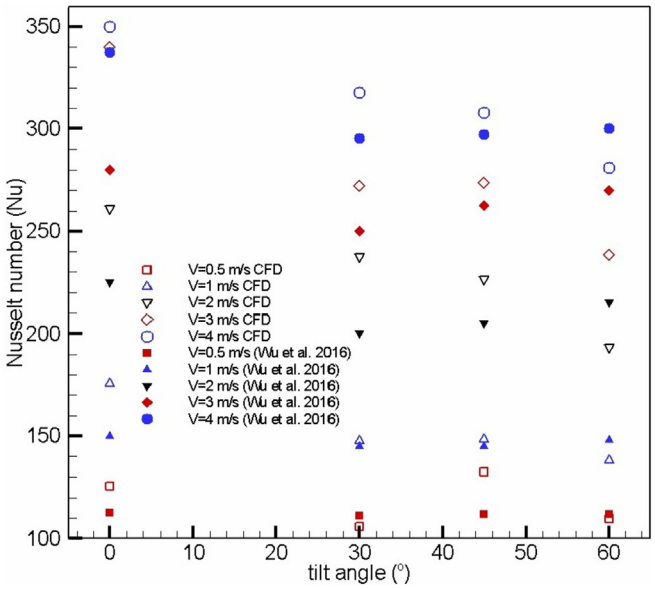

Fig. 6. Nusselt number variation of CFD model (designed dimensionally same as the experimental set up [13]) and literature [13] (see Fig. 1(b)) w.r.t. different tilt angles (θ) of the flat solar collector.

$$C = 365.9\left(1 - 0.00883\,\beta + 0.0001298\,\beta^2\right)$$

M = number of glass covers.

Overall heat loss coefficient (U_l) is given below.

$$U_l = U_s + U_b + U_t \tag{12}$$

In this paper results are presented for $U_l = 0$, which corresponds to ideal condition where heat losses are negligible [10].

Final η_{th} is expressed below as,

$$\eta_{th} = \frac{Q_u}{IA_p} = F_R\left\{(\alpha\tau) - \frac{U_l(T_o - T_i)}{I}\right\} \tag{13}$$

Heat flux applied at the absorber plate, q_i is reduced by a factor $\cos\theta_i$ from the direct solar radiation q_d and given as,

$$q_i = q_d.\cos\theta_i \tag{14}$$

4. Validation of numerical model

The computational model has been validated with the experimental data from the literatures for two different cases are: (a) curved SAH for thermal performance [12] and (b) curved and flat SAH to study the effect of environmental wind condition [13]. Different turbulence models such as K-Epsilon, K-Omega, Spalart-Allmaras and Reynolds-Stress are compared with the experimental data of the literature [12]. The numerical results obtained using K-Epsilon turbulence model shows close match with the experimental data. Interested reader can refer the reference [10] for further details. K-Epsilon turbulence model has been used for further investigation in this paper.

4.1. Validation of curved solar air heater model

In the present study, the heat loss from the top surface of SAH is considered by assigning convection heat transfer, and value of convection heat transfer coefficient has been calculated using equation $h = 5.7 + 3.8V_\infty$ (W/m^{2}K) [26], where atmospheric wind velocity V_∞ has been taken as 3 m/s. Rest surfaces of SAH were kept as adiabatic in the investigation, consequently marginally higher values of the average outlet air temperature have been found compared to experimental data in the literature [12]. The numerical heat transfer analysis has been conducted to predict the impact of flow behavior on heat transfer characteristics. The percentage

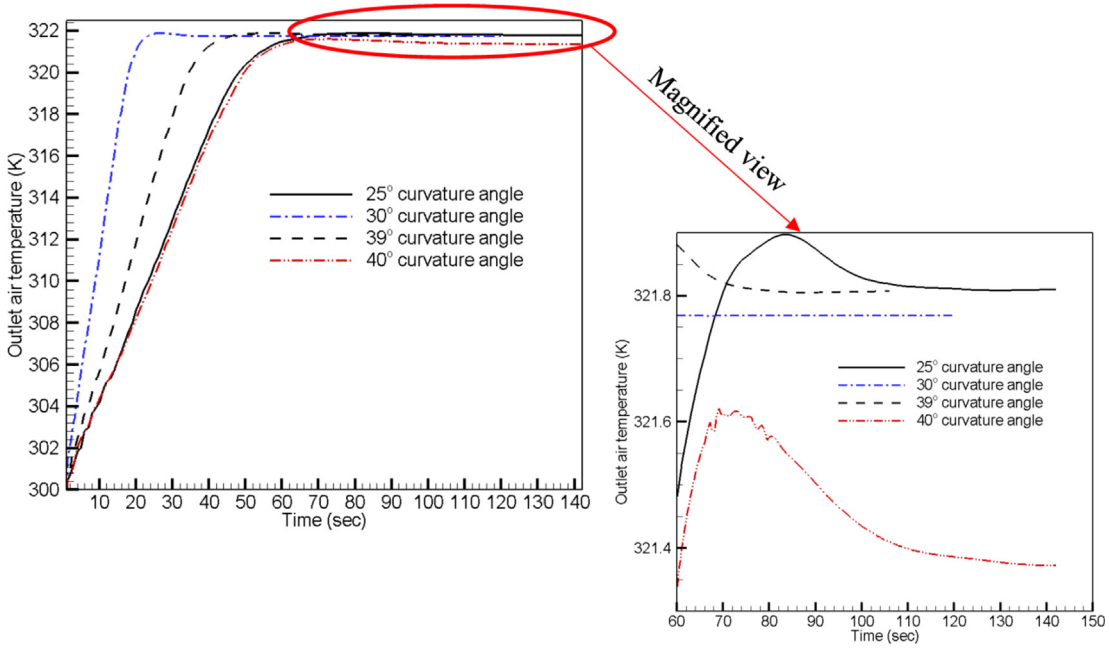

Fig. 7. Major variation of T_o of curved SAH for different curvature angle when the absorber surface exposed to constant heat flux of 800 W/m^2, at fixed value of mass flow rate i.e. 0.0472 kg/sm^2.

deviation of temperature difference between outlet air temperature (T_o) and inlet air temperature (T_i) from numerical model (i.e. $\Delta T_{numerical}$) of curved plate single pass flow (CPSP) SAH with respect to experimental data (i.e. $\Delta T_{exp.}$) of the literature [12] have been seen in the range 1.11–10.19%, 0.5–1.42%, and 6.25–11% for the mass flow rate of 0.0172 (refer Fig. 5(a)), 0.029, and 0.0472 kg/sm^2, respectively. Figures for other mass flow rates has not been shown for brevity. The variation of thermal efficiency of a SAH at different mass flow rates are also compared and range of percentage deviation was found of the order 0.6–9.5% is shown in Fig. 5(b). All simulation results that have been discussed above are in good agreement with the experimental results described in the literature [12].

4.2. Validation of computational model of SAH under environmental wind conditions

The computational model was designed exactly same as the dimensions of experimental setup (see Fig. 1(b)) which has been considered in the literature [13]. Similar boundary conditions were opted to analyze the wind effects on the solar collector model to check the authenticity of CFD model. The results were obtained under constant heat flux of 1200 W/m^2 under different wind velocities for windward position. The values of Nusselt number (Nu) obtained from the simulation found to be more than the experimental results of the literature [13], due to ideal condition of adiabatic walls which does not allow heat loss to surroundings. The

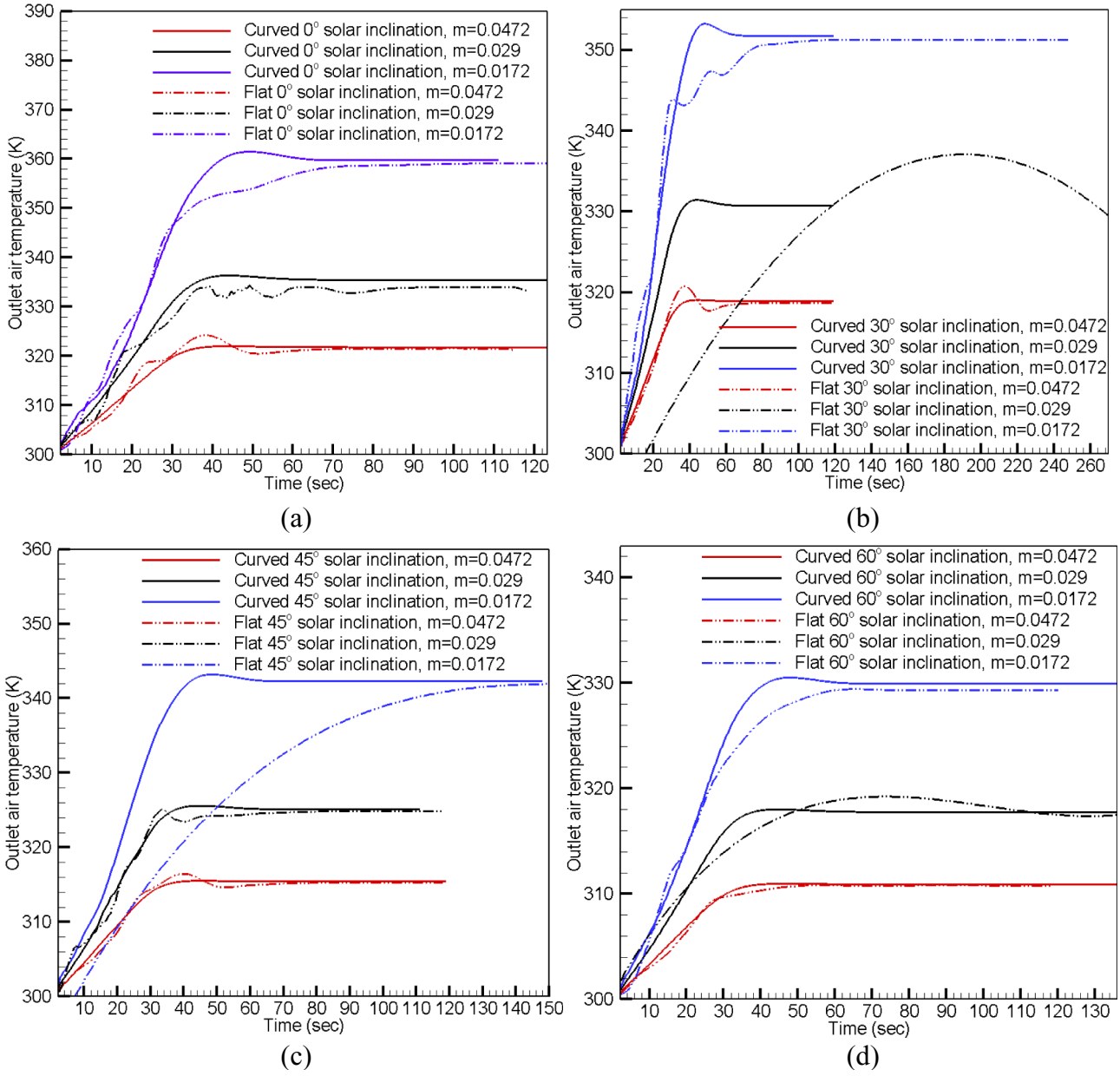

Fig. 8. (a), (b), (c), and (d) shows the variation of outlet air temperature with time when solar radiation inclination angle in range of $\theta_i = 0°–60°$ of curved SAH (25° curvature angle) at different values of mass flow rate (i.e. 0.0172, 0.029 and 0.0472 kg/sm^2).

numerical results shows good agreement with the experimental data has been shown in Fig. 6. The minimum and maximum error incurred are 1.98% and 21.04%, respectively.

5. Results and discussions

5.1. Curved Vs. flat SAH: thermal performance

In this subsection, we first find the optimum curvature angle for which solar heater gives higher thermal efficiency. We then compare the thermal performance of this optimum curved SAH with traditional flat air heater. The internal heat transfer characteristics of curved SAH geometries having curvature angle in the range of 22°–40° were obtained for the three different mass flow rate i.e. 0.0172, 0.029, and 0.0472 kg/s.m^2 at different solar radiation angle (θ_i). The effect of curvature angle of SAH on non-dimensional Nusselt number (Nu), outlet air temperature (T_o) and friction losses (pressure drop) have been discussed in this section. The results have been obtained for all cases and comparisons were made to determine optimum curvature angle of curved SAH. The various effect of environmental wind conditions on SAH were also discussed further in detail in the next section. The air enters at the inlet of curved SAH, air flow smoothly follows the curved passage and finally exit from the outlet section. The centrifugal and centripetal forces comes in picture and plays a very vital role in enhancing heat transfer rate to the air flowing in the SAH duct. At low mass flow rates, centrifugal forces are less intense which does not effects the main velocity profile and consequently formation of small secondary vortices near the absorber plate wall. The increase in the value of mass flow rate i.e. for higher value of Dean number results in increase of centrifugal force, which manifest more velocity gradients and rapid mixing of air near the surface of hot absorber plate [12,24].

5.1.1. Optimum curved angle

The variation of outlet air temperature (T_o), Nusselt number (Nu)

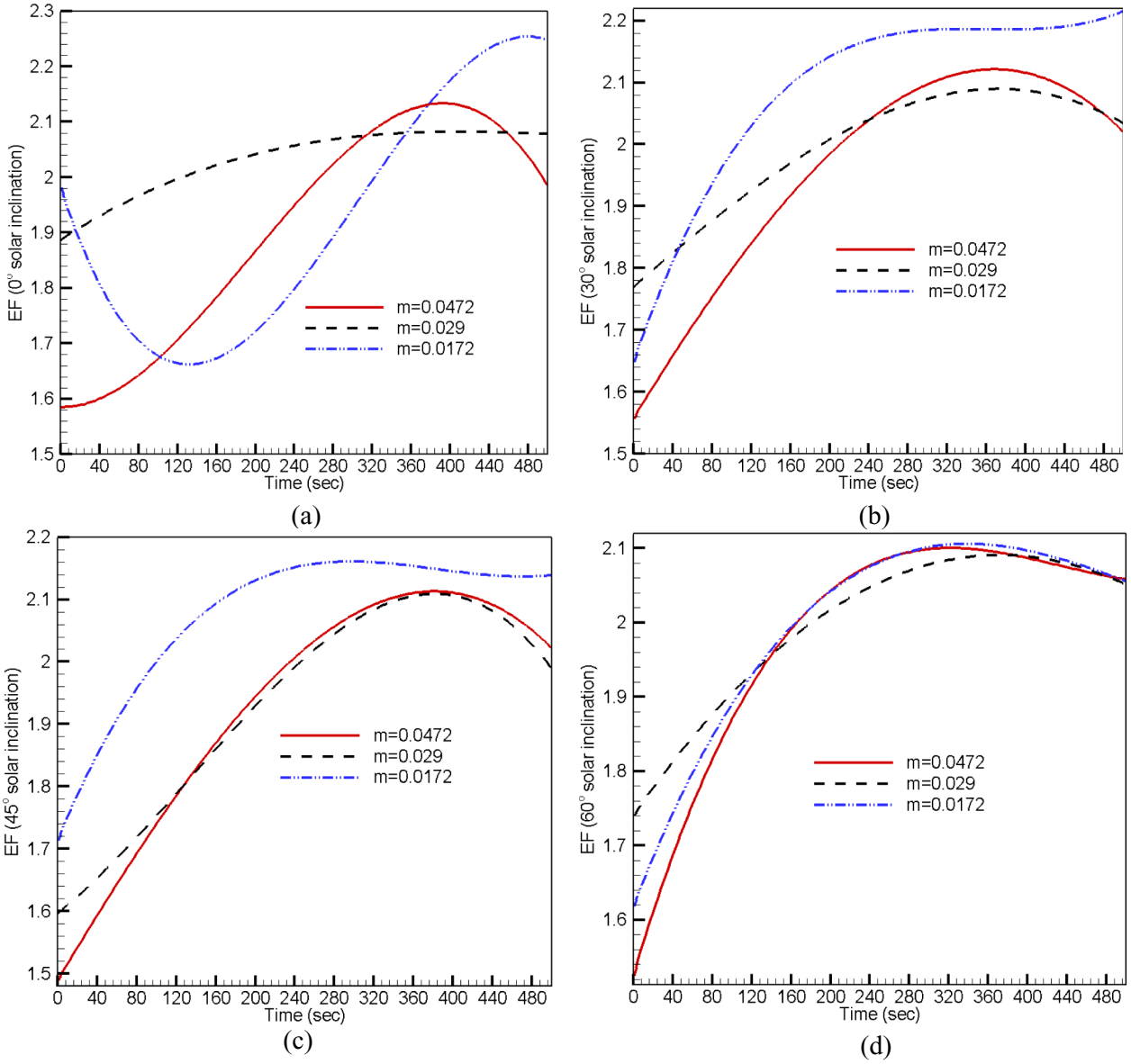

Fig. 9. (a), (b), (c), and (d) shows the variation of heat transfer enhancement factor (EF) with time when solar radiation inclination angle in range of $\theta_i = 0°–60°$ of curved SAH (25° curvature angle) at different values of mass flow rate (i.e. 0.0172, 0.029 and 0.0472 kg/sm^2).

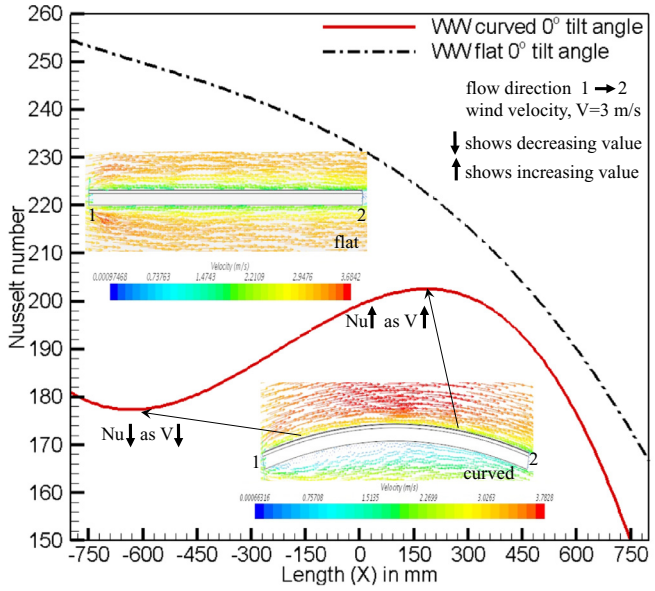

Fig. 10. *Nu* variation for the tilt angle $\theta = 0°$ of curved and flat SAH at wind velocity of 3 m/s.

and pressure drop for all curvature angles in range of 22°–40° of curved SAH have been discussed. Among these results, the parametric variation for different curvature angles which exhibit major variation were shown for the sake of clarity and proper visualization. As mentioned earlier, assessing the transient thermal performance is critical as a SAH has to perform under various conditions such as varying solar radiation. Fig. 7 shows the transient variation of air temperature at the outlet section under constant absorber heat flux of 800 W/m^2 at fixed mass flow rate of 0.0472 kg/s.m^2. During initial seconds, the rate of increase of T_o is maximum for 30° curvature angle but once the steady state attained, the maximum T_o found to be maximum for 25° curvature angle. The pressure drop variation for all curvature angles of curved SAH in range of 22°–40° at three different values of mass flow rate, when the absorber surface exposed to constant heat flux of 800 W/m^2. The minimum value of pressure drop is seen to be associate with 25° curvature angle among the range of 25°–40° for each three different values of mass flow rate, which is an advantage in terms of less power consumption. The pressure drop increases with increasing value of curvature angle of curved SAH due to rise in centrifugal forces results in more resistance to air flow near the absorber wall. The *Nu* variation of a curved SAH having curvature angle in range of 22°–40° at different values of mass flow rate, when the absorber surface exposed to constant heat flux of 800 W/m^2. The maximum value of *Nu* has been found to be maximum for all curvature angles at the mass flow rate of 0.0472 kg/sm^2, followed by 0.029 kg/sm^2 and minimum for 0.0172 kg/sm^2. At lower values of mass flow rate *Nu* is maximum for 25° curvature angle in the range of 22°–33° curvature angle, but after 34° the value of *Nu* increases slightly up to 40° in comparison to 25°. The maximum T_o and minimum friction losses have been observed for curved SAH having 25° curvature angle, and hence chosen for further analysis and evaluation.

5.1.2. Performance comparison: curved vs. flat

The comparison between curved (25° curvature angle) and flat plate SAH under different solar radiation inclination angle (θ_i) in range of 0°–60° w.r.t. normal to the absorber surface (see Fig. 2(a)), for three different values of mass flow rate i.e. 0.0172, 0.029 and 0.0472 kg/sm^2, respectively have been presented in this subsection. The transient variation of T_o was determined for 0°, 15°, 30°, 45° and 60° solar radiation inclination angle and found to be higher for curved SAH compared to flat plate SAH in all cases under same set of boundary conditions as shown in Fig. 8. The air temperature at the outlet section was more for lower mass flow rates due to more exposure time of air with the hot absorber plate of SAH and vice versa for the higher values of mass flow rate. The heat transfer enhancement factor (*EF*) is a factor to represent the heat transfer enhancement of a curved SAH w.r.t. flat plate SAH. The term heat transfer enhancement factor '*EF*' is defined as the ratio of Nusselt number of curved SAH to Nusselt number of flat plate SAH. Fig. 9 shows the variation of *EF* when the absorber surface has been exposed to constant heat flux at specific solar radiation inclination

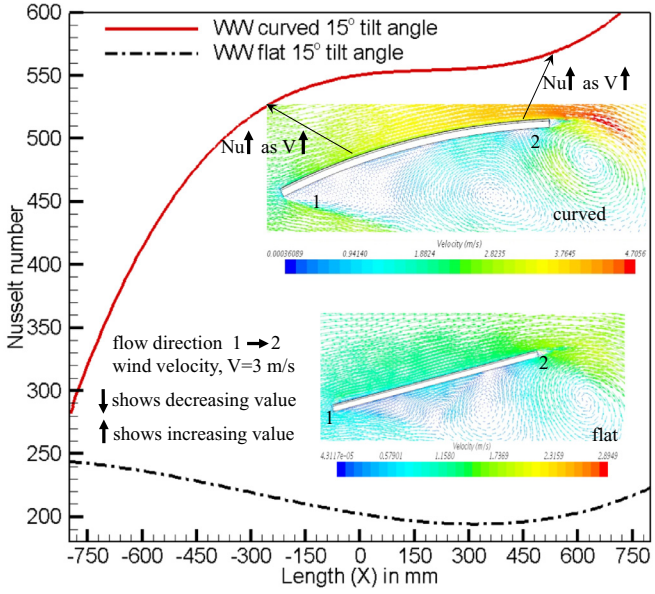

Fig. 11. Nusselt number variation for tilt angle $\theta = 15°$ of curved and flat SAH at wind velocity of 3 m/s in windward position.

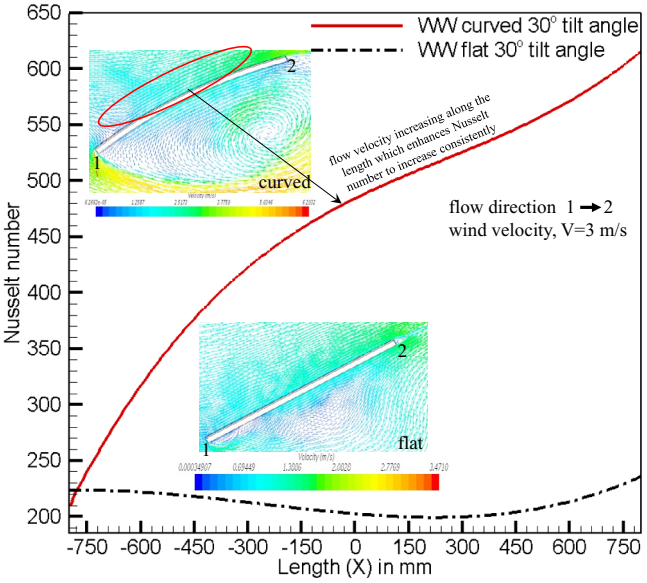

Fig. 12. Nusselt number variation for tilt angle $\theta = 30°$ of curved and flat SAH at wind velocity of 3 m/s in windward position.

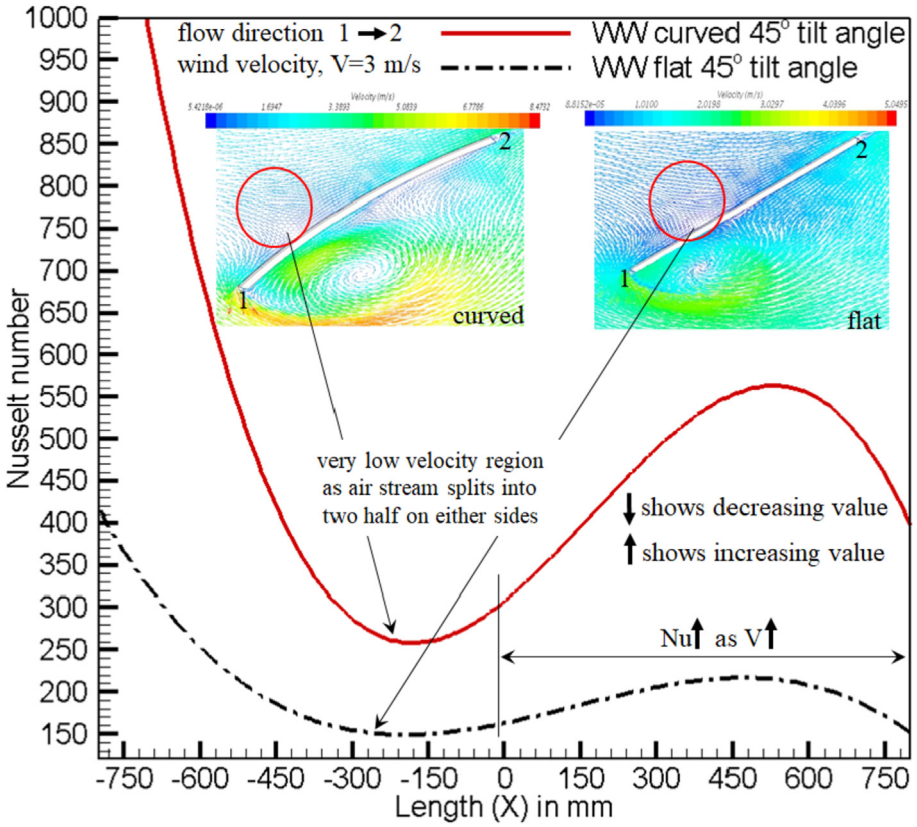

Fig. 13. Nusselt number variation for tilt angle $\theta = 45^{\circ}$ of curved and flat SAH at wind velocity of 3 m/s in windward position.

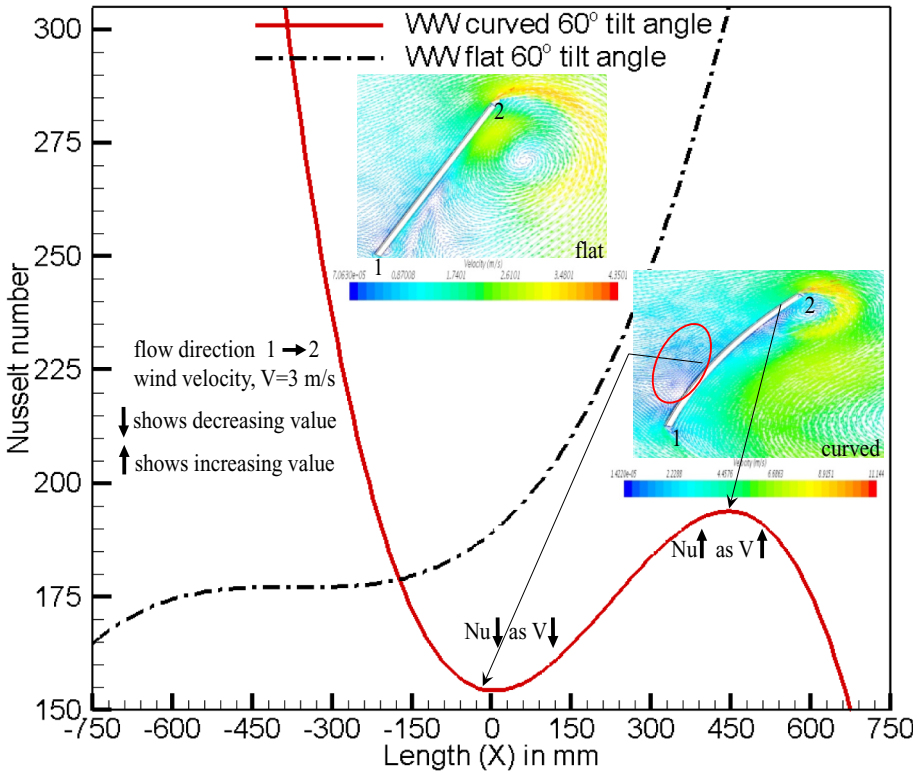

Fig. 14. Nusselt number variation for tilt angle $\theta = 60^{\circ}$ of curved and flat SAH at wind velocity of 3 m/s in windward position.

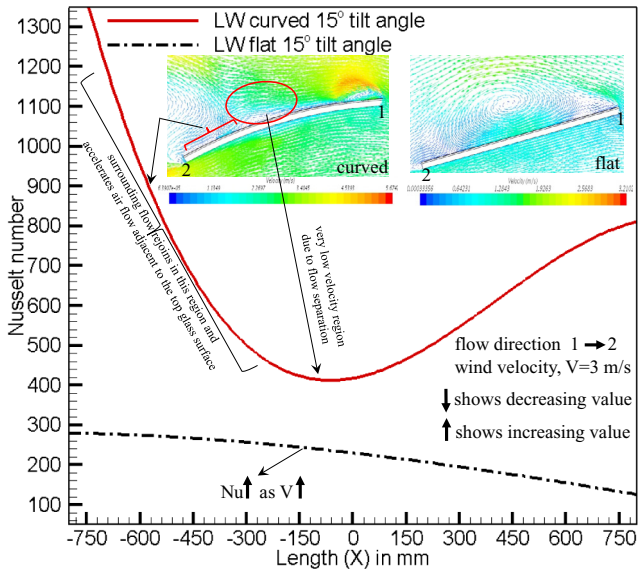

Fig. 15. Velocity contours: (a) curved and (b) flat SAH. (c) Nusselt number variation for tilt angle $\theta = 15°$ of curved and flat SAH at wind velocity of 3 m/s in leeward position.

angle. After steady state, the value of *EF* was found to be slightly more effective for mass flow rate of 0.0172 kg/sm^2 followed by 0.029 kg/sm^2 and minimum for 0.0472 kg/sm^2, for the range of solar radiation inclination angle of 0°–60°. It can be noticed that curved SAH is thermally more efficient in comparison to conventional SAH under same operating conditions.

An economic analysis was performed to estimate the production cost of hot air using flat and curved SAH [27,28]. The productive cost of per kg energy gain of hot air obtained by curved SAH is 0.012 USD ($) per kWh, however it is 0.017 USD ($) per kWh for flat plate SAH. Therefore, per kg production cost of hot air using curved SAH device is about 24% cheaper than flat SAH device. For brevity, detailed economic analysis is not presented here.

* Conversion rate as per 2nd July 2019, 1 USD = 69.0108 INR.

5.2. Curved Vs. flat SAH: heat loss characteristics under environmental wind effect

The steady state Nusselt number variations extracted along the length of a curved SAH at windward and leeward orientation of wind i.e. X*OY and XOY-plane (see Figs. 2(c), 3(b) and (c)), respectively, when wind blows over SAH oriented at different tilt angles in the range of 0°–60° under diverse wind velocities. The variation trend obtained for Nusselt number under the environmental wind velocity of 0.5, 1, 2, 3 and 4 m/s is directly influenced by air flow pattern adjacent to outer surfaces of solar air heater. The variation trend for Nusselt number are similar for all wind velocities at specific tilt angle 'θ' under constant value of absorber heat flux. *The variation of Nusselt number for flat solar collector are in good agreement with experimental results of the literature* [13] (see Fig. 6). The maximum values have been associated with the wind velocity of 4 m/s and minimum values for 0.5 m/s. The aim is to find *Nu* at the top surface of glass (glazing) along the length of SAH associated with blowing air that surrounds the surfaces of air heater, in order to explore the venues of heat loss from top glass surface of SAH to surroundings. The *Nu* variation directly depends on the flow velocity of air and vortices formation adjacent to top surface of glass (glazing) of SAH. The observations for windward and leeward

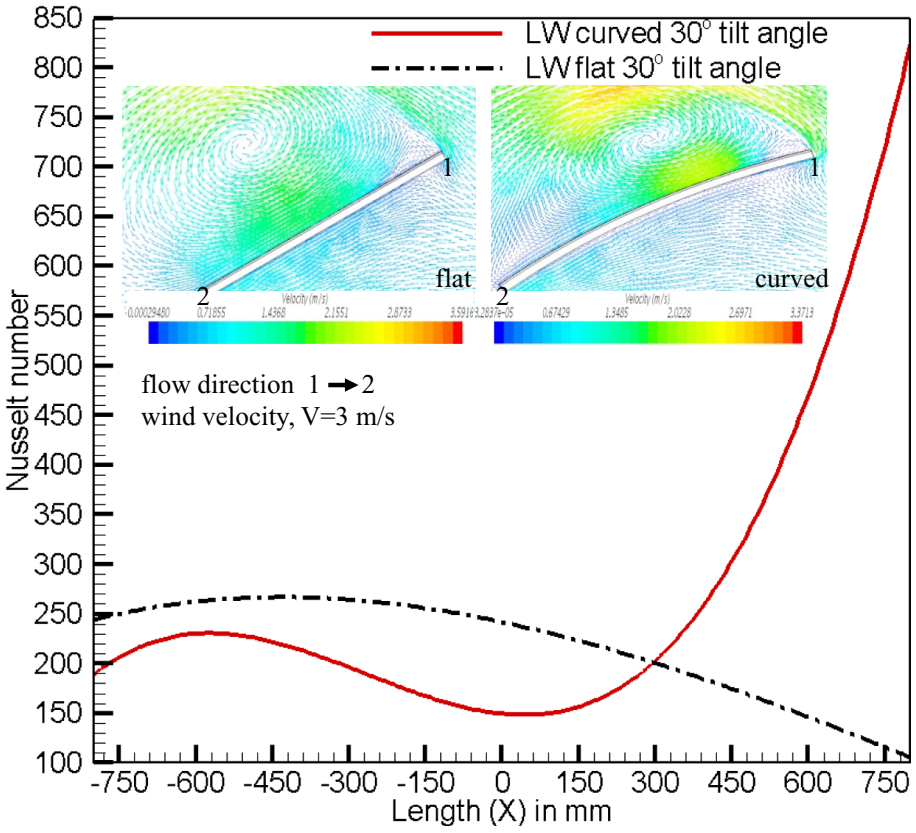

Fig. 16. Velocity contours: (a) curved and (b) flat SAH. (c) Nusselt number variation for tilt angle $\theta = 30°$ of curved and flat SAH at wind velocity of 3 m/s in leeward position.

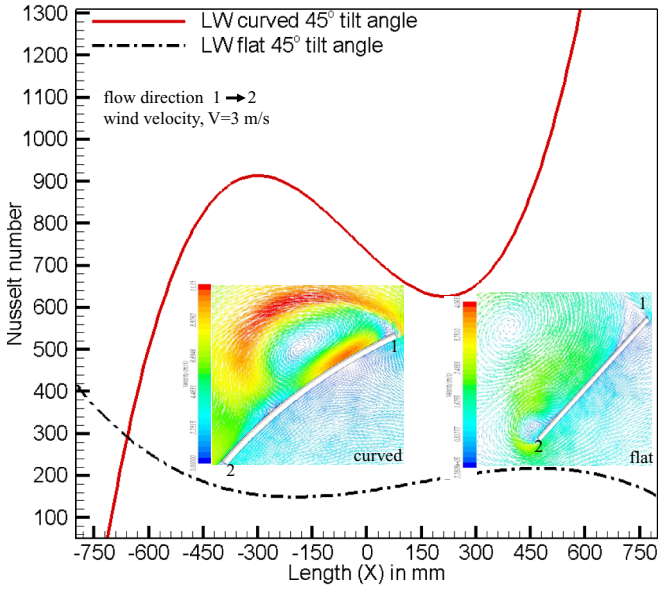

Fig. 17. Velocity contours: (a) curved and (b) flat SAH. (c) Nusselt number variation for tilt angle $\theta = 45°$ of curved and flat SAH at wind velocity of 3 m/s in leeward position.

orientation have been captured and discussed in the sub-sections below.

The Fig. 10, shows the variation of Nusselt number along the length of a curved & flat SAH placed horizontally (0° tilt angle) inside the wind tunnel at wind velocity of 3 m/s. The velocity of air adjacent to top glass (glazing) is gradually decreasing along the length of SAH (see vector contours of curved SAH in the same figure) and the same decreasing trend has been followed by *Nu* (see vector contours of flat SAH). An increase in the values of *Nu* at the mid length is observed in case of flat plate SAH because of more flow velocity. The *Nu* of curved SAH near the trailing edge is less when compared to flat one due to earlier flow separation because of curvature effect. The variation of parameters for 0° tilt angle of SAH were same for both windward and leeward position due to symmetry. The results shown above, revealed that higher values of *Nu* represents more heat loss to surroundings, which abruptly decreases thermal performance of SAH. In above case (0° tilt angle), the *Nu* values for flat SAH are more in comparison to curved SAH, which shows that curved SAH is thermally more efficient under same sets of operating conditions.

5.2.1. Windward orientation

The *Nu* variation directly influenced by movement of air flow at the top glass surface of SAH. The magnified view of velocity contours have been shown in each case for both windward and leeward position. In windward position (see Fig. 3(b)), the similar variation of *Nu* along the length of curved & flat SAH when oriented to tilt angle of $\theta = 15°$ (Fig. 11) & 30° (Fig. 12) located inside the wind tunnel at wind velocity of 3 m/s. The value of *Nu* for a curved SAH continually increases along the length because of higher flow velocity (refer Figs. 11 and 12). The length span of −100 to −650 mm on the negative X-axis (left portion w.r.t. mid) of the curved SAH, a sudden increase has been observed due to curvature effect and hence, higher velocity of air adjacent to the top glass (glazing). A slight decrease in the *Nu* at the first half (negative X-axis) and increasing curve at the second half (positive X-axis) has been observed in case of flat SAH due to absence of curvature effect.

Fig. 13 shows the variation of *Nu* along the length of the curved & flat SAH when set to a tilt angle of $\theta = 45°$ inside the wind tunnel at wind velocity of 3 m/s. A sudden drop was observed at the first half in both curved & flat design because flow directly splashed and splits to up and down stream, which results in a small passive (stagnation) zone and lowers the *Nu* value. The increasing trend of *Nu* has been seen on the positive X-axis, as flow accelerates towards trailing edge.

Fig. 14 demonstrate the variation of *Nu* along the length of a curved & flat SAH when set to a tilt angle of $\theta = 60°$ inside the wind tunnel at wind velocity of 3 m/s. The reason for decrease in *Nu* for SAH at the mid span is same as discussed above in the case of $\theta = 45°$. The heat loss from the curved SAH to environment being less due to lower values of *Nu* compared to flat SAH.

In windward position for tilt angle of 0° and 60°, curved SAH is associated with less heat loss to surroundings as the Nusselt

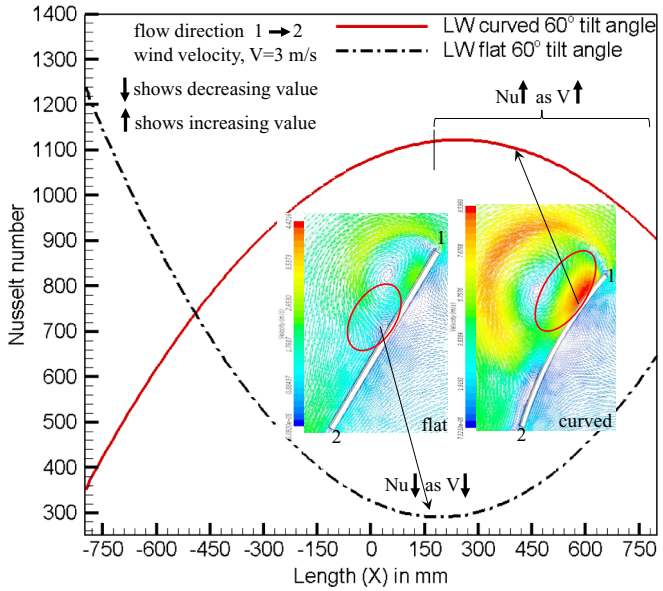

Fig. 18. Velocity contours: (a) curved and (b) flat SAH. (c) Nusselt number variation for tilt angle $\theta = 60°$ of curved and flat SAH at wind velocity of 3 m/s in leeward position.

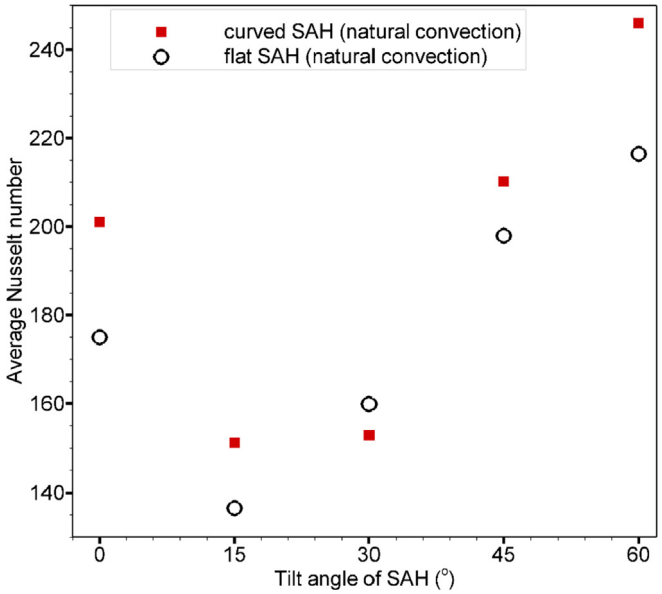

Fig. 19. Average Nusselt number variation of curved and flat SAH at constant absorber heat flux for various tilt angle under natural convection condition.

number values are lower as compared to flat SAH.

5.2.2. Leeward orientation

In the leeward position (see Fig. 3(c)), the vortex formation over the top glass surface (glazing) of a curved SAH has a significant impact on heat transfer [13,14,17]. The variation of *Nu* and velocity contours were obtained for each 'θ' values i.e. 15°, 30°, 45° and 60°, of the curved and flat SAH placed inside the wind tunnel. At $\theta = 15°$ (see Fig. 15), the *Nu* values for curved SAH suddenly drop near mid span due to adverse velocity gradients. The increasing values of *Nu* in case of curved SAH can be seen as the flow accelerates towards trailing edge at the negative X-axis.

In case, $\theta = 30°$ (see Fig. 16), the *Nu* for curved SAH has been found to be lower in comparison to flat SAH after some distance from the leading edge because of flow separation which is reflected in less heat loss associated with curved SAH to surroundings. In case, $\theta = 45°$ (see Fig. 17), vortex formation starts from the leading edge itself and sustained up to mid of curved SAH which finally rejoins with the air flowing adjacent to top glass at the middle. This phenomenon accelerates the flow from the mid span towards trailing edge (i.e. negative X-axis). The *Nu* follows the same trend, decreasing at the first half and increasing at the second half in both the cases ($\theta = 30°$ & $\theta = 45°$) as discussed above.

In case of $\theta = 60°$ (see Fig. 18) for curved SAH, the flow velocity is increasing from the leading edge up to one-fourth portion, due to intense mixing in the swirl region and, consequently increasing values of *Nu* can be seen. The swirl flow past the latter half portion of curved SAH and around one-third distance from the leading edge in case of flat SAH, flow splits into two streams (refer Fig. 18) moving opposite to each other. The point where the flow splits into two streams creates a slow moving zone whose effect can be seen in the sudden drop in the values of *Nu* in the zone near trailing edge (i.e. on negative X-axis) in case of curved SAH and one-third portion from the leading edge in case of flat SAH. The *Nu* increases at the later (second) half portion up to trailing edge in all cases of flat plate SAH for leeward position. The increasing values of *Nu* is basically due to vortex formation which consequently enhances the mixing of air adjacent to the top glass surface. Figs. 15–18 for the case of flat SAH for leeward position, flow of air adjacent to top glass surface is accelerating due to vortex generation which provides scope of good mixing of air in the flow for all values of 'θ'.

In leeward position for tilt angle of 0° and 30°, curved SAH is

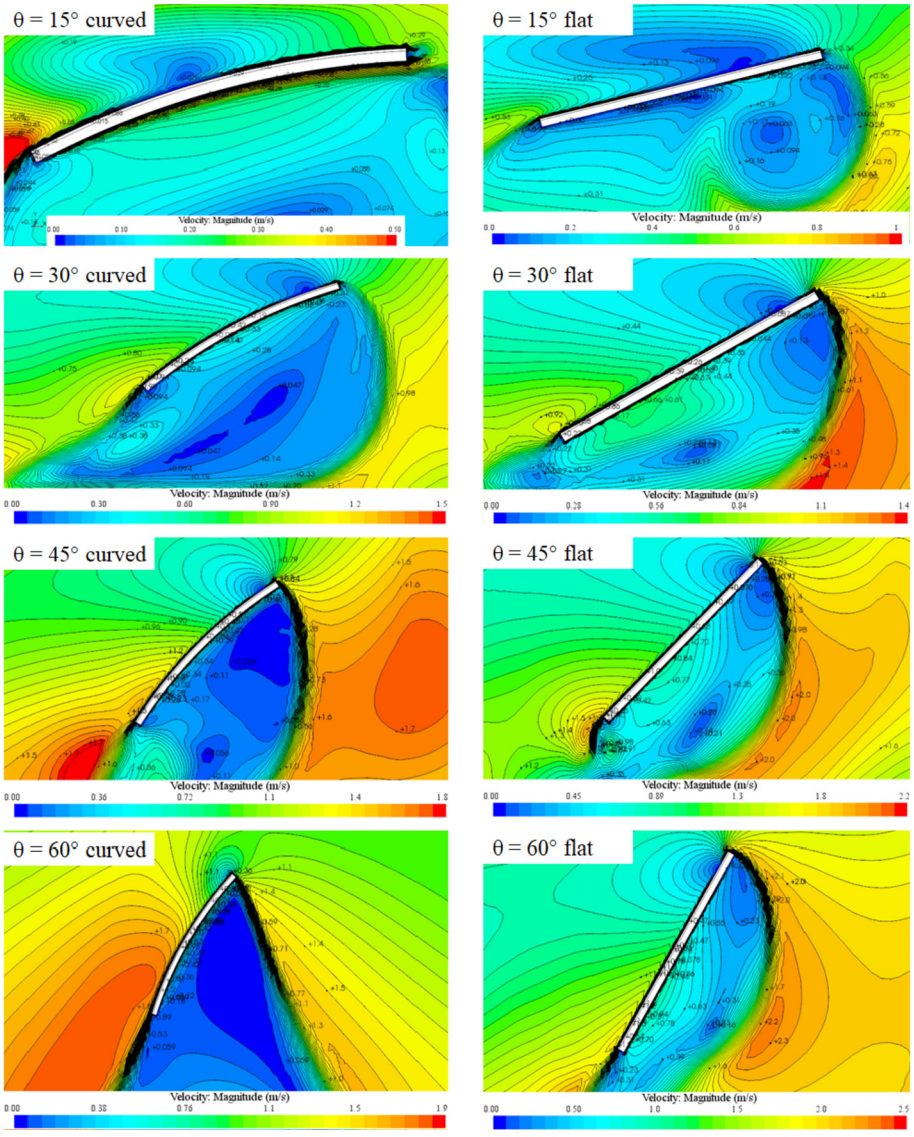

Fig. 20. Velocity contours of curved and flat SAH at various tilt angle ($\theta = 15°$, 30°, 45° and 60°) under natural convection condition.

associated with less heat loss to surroundings as the *Nu* values are lower as compared to flat SAH.

5.2.3. Performance under natural convection (standstill air environment)

There are situations when the environmental air velocity over the solar air heater is extremely slow. In the extreme limit of no flow condition (natural convection), thermal characteristics at various tilt angle of curved vs. flat SAH is not well documented in the scientific literature. Fig. 19 demonstrates the variation of average Nusselt number for a curved and flat SAH at various tilt angle under natural convection. The tilt angle 15°, act as an inversion point as the average *Nu* values increases on the either side for both curved and flat SAH. The average *Nu* values for curved SAH have been found to be slightly higher than the flat SAH, except for 30° tilt angle. This happens due to the area of passive zone (slow moving flow) formation near the extreme right end of flat SAH is more than the curved SAH, which can be seen in velocity contours in Fig. 20. The curved geometry of curved SAH offers more exposure to air flow and possess more velocity at the top glass surface compared to flat one (refer Fig. 20). At extreme ends of curved SAH where flow vortices frequently formed and interact with the top glass surface, consequently increases the Nusselt number. The average *Nu* is maximum for tilt angle 60° due to more flow velocity and frequent mixing in the flow at the top glass surface of SAH. The heat loss associated with curved SAH has been slightly higher than flat SAH. Hence in case of standstill or tranquil wind condition, flat SAH losses less heat to surroundings in comparison to curved SAH.

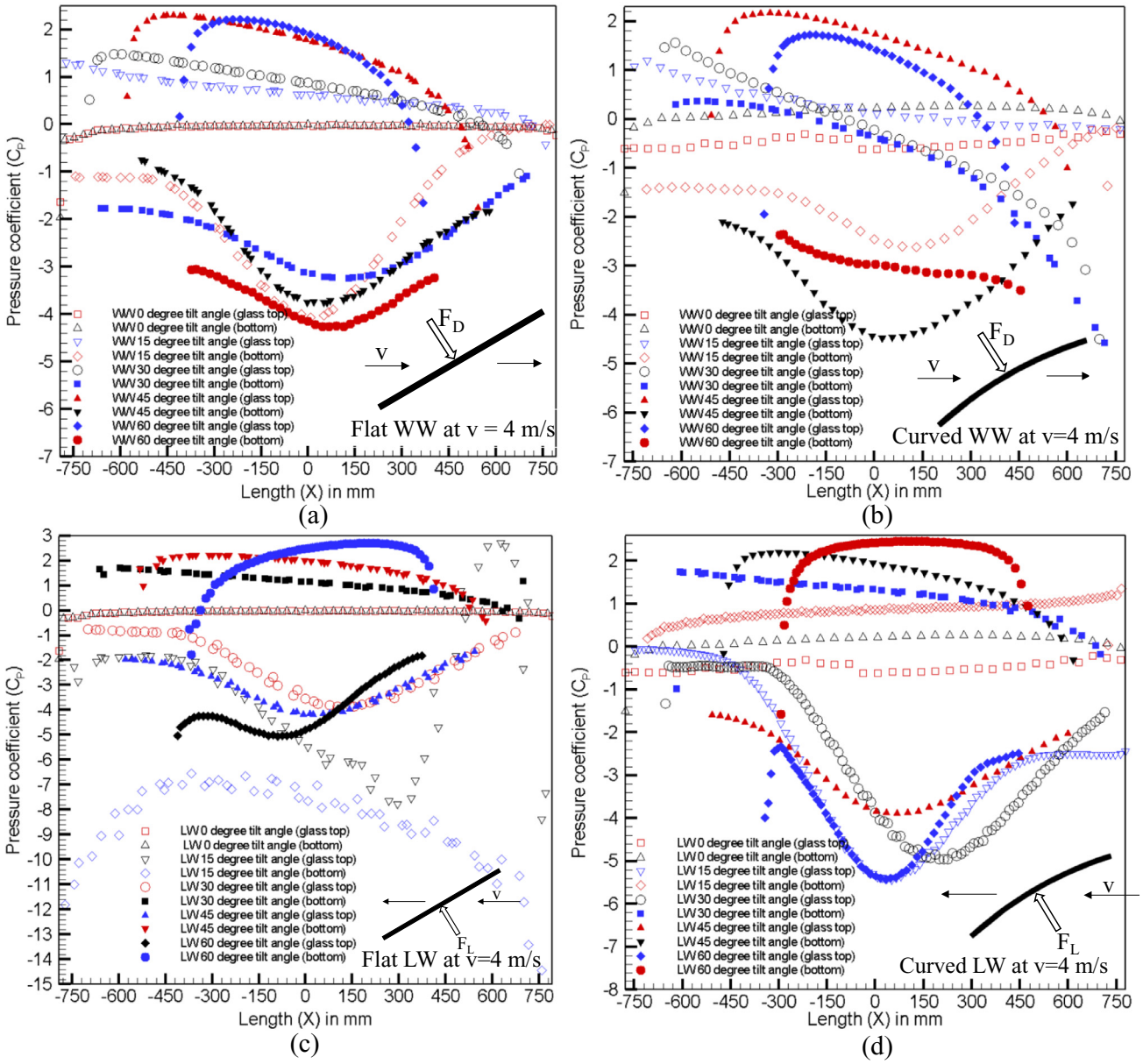

Fig. 21. Pressure coefficient (C_P) variation at the top and bottom surface of flat and curved SAH for various SAH tilt angle at wind velocity (v) of 4 m/s: (a) flat SAH at windward position (b) curved SAH at windward position; (c) flat SAH at leeward position; (d) curved SAH at leeward position. Insert in the figures shows wind direction and net force acting on the SAH, F_L denotes net lift force and F_D denotes net downward force.

Table 5
Range of C_P for curved and flat SAH in windward position.

Curved SAH	C_P range on top glass at windward position				
wind velocity (m/s) ⬇	0°	15°	30°	45°	60°
0.5	2.15–2.49	2.23–3.89	3.85–6.52	5.20–8.29	6.72–10.69
1	2.09–2.48	1.42–3.92	−2.67–7.12	2.48–9.26	−0.30–10.01
2	−1.74–−0.05	−0.32–1.36	−4.10–1.79	−1.29–3.11	−1.88–2.52
3	−3.99–2.58	−2.11–1.93	−6.14–1.56	0.03–1.48	−1.89–−0.19
4	−1.91–−0.20	−0.24–1.19	−5.62–1.57	−2.53–2.16	−3.05–1.72
C_P range on bottom surface at windward position					
wind velocity (m/s) ⬇	**0°**	**15°**	**30°**	**45°**	**60°**
0.5	2.28–2.67	2.41–3.52	4.10–5.49	5.22–6.75	6.34–9.68
1	2.30–2.69	−1.09–1.85	−3.02–5.70	1.99–7.33	−1.18–8.21
2	−1.33–0.41	−3.06–−0.06	−3.40–0.24	−3.24–0.60	−2.37–−1.52
3	−1.48–0.27	−2.95–0.11	−5.80–0.24	−4.35–−1.25	−5.01–−1.41
4	−1.49–0.26	−2.62–−0.15	−4.83–0.36	−4.48–−1.64	−3.64–−2.35
Flat SAH	C_P range on top glass at windward position				
wind velocity (m/s) ⬇	**0°**	**15°**	**30°**	**45°**	**60°**
0.5	2.21–2.57	2.32–4.21	3.88–6.78	4.47–8.59	7.21–10.53
1	0.60–2.19	2.32–4.88	1.98–7.22	1.52–8.28	−0.89–11.62
2	−0.66–0.05	−0.40–1.46	−1.38–1.87	−1.46–2.86	−3.18–3.77
3	−1.61–0.01	−0.41–1.38	−1.32–1.47	−1.49–2.13	−2.71–2.31
4	−1.62–0.002	−0.42–1.39	−1.03–1.48	−1.75–2.29	−2.92–2.21
C_P range on bottom surface at windward position					
wind velocity (m/s) ⬇	**0°**	**15°**	**30°**	**45°**	**60°**
0.5	2.22–2.71	2.31–3.74	4.11–6.44	3.98–7.47	3.86–7.09
1	0.41–2.34	−0.59–2.57	0.66–4.91	0.78–5.40	−2.59–8.89
2	−0.79–0.07	−0.14–−3.52	−3.66–−0.83	−3.81–0.48	−5.07–−0.77
3	−1.92–0.02	−3.80–−0.07	−2.94–−1.30	−3.62–−1.35	−4.39–−2.54
4	−1.94–0.006	−4.11–−0.003	−3.24–−1.09	−3.77–−0.74	−4.27–−3.04

5.3. Curved Vs. flat SAH: aerodynamic characteristics

5.3.1. Longitudinal pressure distribution

The pressure force exerted by the environmental wind on the solar air heater is a very important factor to study while installing solar collectors for the sake of device structural integrity [15–17]. The expression for coefficient of pressure (C_P) is the relation among dimensionless coefficient and the dimensionless number to study the fluid flow. The expression is provided below:

$$C_P = \frac{(P - P_\infty)}{\frac{1}{2}\rho_\infty V_\infty^2}, \tag{15}$$

where P is the static pressure at the point where C_P is being measured, ρ_∞ is the fluid density of the free stream, P_∞ is the static pressure of free stream, and V_∞ is the velocity of free stream.

In fluid dynamics, the Mach number (M) is a dimensionless quantity, which is the ratio of the flow velocity past a boundary 'V' to the local speed of sound 'c' (i.e. $M = \frac{V}{C}$). In the present study, the wind velocity is in the range of 0.5–4 m/s, the corresponding value of Mach number always be less than 0.3 ($M < 0.3$). The flow is treated as incompressible throughout the study as the M is less than 0.3. Hence, the above coefficient of pressure formula is valid for our analysis.

The streamwise differential pressure coefficient i.e. ΔC_P plays vital role in wind loading given as:

$$C_{P/t} = \frac{(P_t - P_\infty)}{\frac{1}{2}\rho_\infty V_\infty^2}, \quad C_{P/b} = \frac{(P_t - P_\infty)}{\frac{1}{2}\rho_\infty V_\infty^2}, \quad \Delta C_P = \frac{(P_t - P_b)}{\frac{1}{2}\rho_\infty V_\infty^2}; \tag{16}$$

where P_t and P_b are pressure at the top glass surface and bottom insulated surface, respectively.

The zero value of C_P indicates the pressure is same as the free stream pressure. The value of C_P is one corresponds to stagnation pressure and indicates the stagnation point. The zero and negative values corresponds to cavitation state or low pressure zone, while non-cavitation state for positive values of C_P. The range of pressure coefficient for all cases along the length of the curved and flat SAH have been determined at the top (glass) and bottom (insulation) surfaces for five different wind velocities i.e. 0.5, 1, 2, 3 and 4 m/s, respectively.

At windward position (refer Fig. 21(a) and (b)), the pressure force is more at the top glass surface when compared to the bottom insulated surface of solar air heater. The air flow directly strikes the top glass surface and formation of flow vortices at the extreme edges (leading and trailing edges) continues towards downstream. The adverse pressure gradient (negative pressure) zone has been created at the bottom surface. Consequently, the values of streamwise differential pressure coefficient (ΔC_P) will be positive, it means the net pressure force exerts in the downward direction which increases the stability against blowing wind [15,17].

The values of C_P of the top glass surface and insulated bottom surface of curved and flat SAH in windward position is shown in

Table 6
Range of C_P for curved and flat SAH in leeward position.

Curved SAH	C_P range on top glass at leeward position				
wind velocity (m/s) ⬇	**0°**	**15°**	**30°**	**45°**	**60°**
0.5	2.15–2.49	0.99–3.27	4.38–5.42	5.49–7.46	5.42–10.20
1	2.09–2.48	−0.77–3.06	2.59–5.25	2.09–5.63	2.52–6.59
2	−1.74–−0.05	−3.64–0.01	−5.03–0.31	−1.71–0.03	−2.69–−0.60
3	−3.99–2.58	−4.79–−0.11	−4.23–−0.48	−3.77–−2.85	−4.77–−1.92
4	−1.91–−0.20	−5.44–−0.05	−4.95–−0.43	−3.90–−1.58	−5.43–−2.29
***C_P* range on bottom surface at leeward position**					
wind velocity (m/s) ⬇	**0°**	**15°**	**30°**	**45°**	**60°**
0.5	2.28–2.67	2.59–3.45	4.78–6.11	5.93–8.06	7.14–10.55
1	2.30–2.69	3.46–4.14	5.80–7.14	4.14–6.98	6.47–9.61
2	−1.33–0.41	0.31–1.71	0.73–2.37	0.92–3.28	−1.31–2.00
3	−1.48–0.27	0.00–1.22	−0.36–1.82	−1.91–1.33	−2.12–2.36
4	−1.49–0.26	0.03–1.35	−0.98–1.74	−1.09–2.18	−1.57–2.45
Flat SAH	C_P range on top glass at leeward position				
wind velocity (m/s) ⬇	**0°**	**15°**	**30°**	**45°**	**60°**
0.5	2.21–2.57	1.27–2.02	4.41–6.26	5.48–7.41	7.14–9.55
1	0.60–2.19	0.14–2.20	2.03–4.56	−1.37–8.30	−2.79–8.08
2	−0.66–0.05	−8.82–0.01	−2.99–−0.58	−1.80–0.18	−5.57–−0.77
3	−1.61–0.01	−2.56–−0.71	−2.88–−1.88	−3.84–−2.74	−7.08–−1.66
4	−1.62–0.002	−8.39–2.70	−3.86–−0.75	−4.18–−1.65	−5.05–−1.81
***C_P* range on bottom surface at leeward position**					
wind velocity (m/s) ⬇	**0°**	**15°**	**30°**	**45°**	**60°**
0.5	2.22–2.71	1.76–2.18	4.82–6.40	5.68–7.83	7.49–10.04
1	0.41–2.34	2.24–2.50	4.36–6.40	3.22–9.52	1.31–9.37
2	−0.79–0.07	0.50–3.23	−0.11–1.69	0.87–3.28	−3.00–4.15
3	−1.92–0.02	−0.06–6.96	−1.45–1.29	−1.81–1.33	−4.80–2.85
4	−1.94–0.006	−3.06–−6.43	−0.56–1.68	−0.74–2.19	−3.39–2.69

Table 5. The values of C_P of the top glass and insulated bottom surface of flat and curved SAH in windward position at wind velocity of 4 m/s have been shown in Fig. 21 (a) and (b), respectively. Please refer the Table 5 for C_P values for other wind velocities. In windward position, the value of ΔC_P increases with increasing values of tilt angle of SAH, since the pressure exerted by the air is more at the top glass surface compared to insulated bottom surface. This phenomenon increases the net downward force (F_D) which becomes more advantageous from the stability point of view.

In Fig. 21 (c) and (d), represents case for leeward position, the pressure force is more at the bottom insulated surface than the top glass surface of solar air heater. The air flow directly strikes the bottom insulated surface and flow vortices at the extreme edges (leading and trailing edges) continues to downstream. The adverse pressure gradient (negative pressure) zone has been created at the top glass surface of SAH. The streamwise differential pressure coefficient (ΔC_P) will yield negative values, it means the net uplift force exerts by the blowing wind in the upward direction (against gravity) which needs more firm clamps to gain enough rigidity to hold the SAH at desired position [15,17]. The values of C_P of the top glass surface and insulated bottom surface of curved and flat SAH for wind velocity of range 0.5–4 m/s in leeward position is shown in Table 6. The values of local pressure coefficient (C_P) for the top glass surface and insulated bottom surface of flat and curved SAH in leeward position at wind velocity of 4 m/s have been shown in Fig. 21 (c) and (d), respectively. In leeward position, the value of ΔC_P decreases with increasing values of tilt angle of SAH, since the pressure exerted by the air is more at the insulated bottom surface compared to top glass surface. This phenomenon increases the net lift force (F_L) in upward direction as tilt angle increases, which needs additional clamps and supports to keep the SAst generated lift force.

The percentage change in average ΔC_P is calculated as $(\Delta C_{P,\ curved} - \Delta C_{P,\ flat})/\Delta C_{P,\ flat}$. In the extreme case of 60° title angle, wind speed of 4 m/s, and windward condition, it is 2.18% higher in curved SAH while it is 18.5% less in leeward condition. This may be due to lower projected area in case of curved SAH and same solar collector surface area for curved and flat heaters.

6. Conclusion

In this paper, we have reported the performance of an optimized curved solar air heat and systematically compared its various characteristics such as thermal performance, environmental heat loss and aerodynamic characteristics with the conventional flat plat SAH. The parameters range investigated are: curvature angle (22–40°), tilt angle of SAH (0–60°), environment heat loss characteristics for both windward and leeward (velocity range: 0–4 m/s) and aerodynamic characteristics (0.5–4 m/s). In the range of parameters used, curved SAH was observed to more efficient than convectional flat SAH. We hope that the data reported in the paper would be beneficial to the scientific community in design and development of better solar air heaters for harnessing sun's energy in efficient ways.

Some specific observations are enumerated below:

(a) A curved solar air heat with curvature angle of 25° shows higher thermal efficiency associate with lower pressure drop. It was observed that heat content in terms of outlet air temperature is maximum for the curved SAH with 25°.
(b) For a given mass flow rate at different solar inclination angle, the value of heat transfer enhancement factor, *EF* (ratio of $Nu_{curved,\ 25^\circ}$ to Nu_{flat}) was observed to always greater than unity in the range of parameters used.
(c) For 0°, 60° (for windward condition) and 30° (for leeward condition) during windy condition, heat loss to surrounding is less for curved SAH compared to flat SAH. For rest of the tilt angle, flat plate SAH shows less heat loss characteristics and hence, better than curved SAH.
(d) Under natural convection condition, environmental heat losses are higher in curved SAH in comparison to flat plate heater except for one tilt angle. Clearly, curved SAH performs poorly under natural convection. However, this higher heat losses are compensated by its better thermal performance in comparison to flat plate SAH.
(e) Aerodynamic performance is compared between the two SAH with same solar collector areas. In the extreme case of 60° title angle, maximum wind speed of 4 m/s, flat plate performs slightly better than curved SAH in windward condition, while in leeward condition, curved design experiences comparatively less lift forces.

References

[1] A.S. Yadav, M.K. Thapak, Artificially roughened solar air heater: experimental investigation, Renew. Sustain. Energy Rev. 36 (2014) 370–411.
[2] L. Li, M. Qu, S. Peng, Performance evaluation of building integrated solar thermal shading system: active solar energy usage, Renew. Energy 109 (2017) 576–585.
[3] R. Mateus, S.M. Silva, M.G.D. Almeida, Environmental and Cost Life Cycle Analysis of the Impact of Using Solar Systems in Energy Renovation of Southern European Single-Family Buildings, Renewable Energy 137 (2019) 82–92.
[4] T.S. Ge, R.Z. Wang, Z.Y. Xu, Q.W. Pan, S. Du, X.M. Chen, T. Ma, X.N. Wu, X.L. Sun, J.F. Chen, Solar heating and cooling: present and future development, Renew. Energy 126 (2018) 1126–1140.
[5] A. Allouhi, T. Kousksou, A. Jamil, T.E. Rhafiki, Y. Mourad, Y. Zeraouli, Economic and environmental assessment of solar air-conditioning systems in Morocco, Renew. Sustain. Energy Rev. 50 (2015) 770–781.
[6] A.M. Baniyounes, Y.Y. Ghadi, M.G. Rasul, M.M.K. Khan, An overview of solar assisted air conditioning in Queensland's subtropical regions, Australia, Renew. Sustain. Energy Rev. 26 (2013) 781–804.
[7] S. Rosiek, F.J. Batlles, Integration of the solar thermal energy in the construction: analysis of the solar-assisted air-conditioning system installed in CIESOL building, Renew. Energy 34 (2009) 1423–1431.
[8] M. Shan, T. Yu, X. Yang, Assessment of an integrated active solar and air-source heat pump water heating system operated within a passive house in a cold climate zone, Renew. Energy 87 (2016) 1059–1066.
[9] K.F. Fong, C.K. Lee, T.T. Chow, Z. Lin, L.S. Chan, Solar hybrid air-conditioning system for high temperature cooling in subtropical city, Renew. Energy 35 (2010) 2439–2451.
[10] A.P. Singh, O.P. Singh, Performance enhancement of a curved solar air heater using CFD, Sol. Energy 174 (2018) 556–569.
[11] S. Singh, Performance evaluation of a solar air heater with arched absorber plate, Renew. Energy 114 (2017) 879–886.
[12] C. Mahboub, N. Moummi, A. Brima, A. Moummi, Experimental study of new solar air heater design, Int. J. Green Energy 13 (2016) 521–529.
[13] S.Y. Wu, H. Zhang, L. Xiao, Y. Qiu, Experimental investigation on convection heat transfer characteristics of flat plate under environmental wind condition, Int. J. Green Energy 14 (2017) 317–329.
[14] T. Stathopoulos, I. Zisis, E. Xypnitou, Local and overall wind pressure and force coefficients for solar panels, J. Wind Eng. Ind. Aerodyn. 125 (2014) 195–206.
[15] A.M. Aly, On the evaluation of wind loads on solar panels: the scale issue, Sol. Energy 135 (2016) 423–434.
[16] M.K. Zemler, G. Bohl, O. Rios, S.K.S. Boetcher, Numerical study of wind forces on parabolic solar collectors, Renew. Energy 60 (2013) 498–505.
[17] K.M. Chung, K.C. Chang, C.C. Chou, Wind loads on residential and large-scale solar collector models, J. Wind Eng. Ind. Aerodyn. 99 (2011) 59–64.
[18] C.R. Chu, S.J. Tsao, Aerodynamic loading of solar trackers on flat-roofed buildings, J. Wind Eng. Ind. Aerodyn. 175 (2018) 202–212.
[19] M. Andre, M. Pentek, K.U. Bletzinger, R. Wuchner, J. Wind Eng. Ind. Aerodyn. 165 (2017) 67–78.
[20] J. Paetzold, S. Cochard, D.F. Fletcher, A. Vassallo, Wind engineering analysis of parabolic trough collectors to optimise wind loads and heat loss, Energy Procedia 69 (2015) 168–177.
[21] G.T. Bitsuamlak, A.K. Dagnew, J. Erwin, Evaluation of wind loads on solar panel modules using CFD, in: International Symposium on Computational Wind Engineering, 2010.
[22] I.H. Yilmaz, A. Mwesigye, Modeling, simulation and performance analysis of parabolic trough solar collectors, Appl. Energy 225 (2018) 135–174.
[23] A.A. Hachicha, I. Rodriguez, A. Oliva, Wind speed effect on the flow and heat transfer around a parabolic trough solar collector, Appl. Energy 130 (2014) 200–211.
[24] N. Nivedita, P. Ligrani, I. Papautsky, Dean flow dynamics in low-aspect ratio spiral microchannels, Sci. Rep. 7 (2017) 1–10.
[25] J.A. Duffie, W.A. Beckman, Solar Engineering of Thermal Processes, fourth ed., John Wiley & Sons, New York, 2013.
[26] S.P. Sukhatme, J.K. Nayak, Principles of Thermal Collection and Storage, third ed. McGraw Hill Education, New Delhi, India.
[27] A.K. Raj, M. Srinivas, S. Jayaraj, A cost-effective method to improve the performance of solar air heaters using discrete macro-encapsulated PCM capsules for drying applications, Appl. Therm. Eng. 146 (2019) 910–920.
[28] A.A. Razak, Z.A.A. Majid, F. Basrawi, A.F. Sharol, M.H. Ruslan, K. Sopian, A performance and technoeconomic study of different geometrical designs of compact single-pass cross-matrix solar air collector with square-tube absorbers, Solar Energy 178 (2019) 314–330.
[29] A.P. Singh, O.P. Singh, Thermo-hydraulic performance enhancement of convex-concave natural convection solar air heaters, Sol. Energy 183 (2019) 146–161.